Hindawi
Journal of Food Processing and Preservation
Volume 2024, Article ID 5887654, 18 pages
https://doi.org/10.1155/2024/5887654

*Research Article*

# Probabilistic-Mechanistic Evaluation of a Hybrid Drying System Using $l_1$ Norm Regularisation: Simultaneous Ohmic Heating and Convection Drying

**Sebahattin Serhat Turgut**,[1,2] **Erdogan Kucukoner**,[1] **Erkan Karacabey**,[1] **and Aberham Hailu Feyissa**[2]

[1]*Department of Food Engineering, Faculty of Engineering and Natural Sciences, Suleyman Demirel University, Isparta, Türkiye*
[2]*Research Group for Food Production Engineering, National Food Institute, Technical University of Denmark (DTU), Kongens Lyngby, Denmark*

Correspondence should be addressed to Sebahattin Serhat Turgut; sebtur@food.dtu.dk

Received 29 October 2022; Revised 21 October 2023; Accepted 20 December 2023; Published 18 January 2024

Academic Editor: Bhupendra M Ghodki



Ohmic-assisted drying (OAD) is a novel drying system that combines ohmic heating and convection drying simultaneously. The present study is aimed at evaluating the mechanism of OAD system behaviours against the combined impact of operational and model uncertainties. Moreover, the dynamic (time-dependent), as well as static (end-of-drying) spatial homogeneity of the model predictions, was quantitatively described for the first time in the literature using Buzas and Gibson's evenness value (an $\alpha$-diversity index). The Monte Carlo simulation approach was used to propagate the uncertainty of randomly selected input variables using the Halton sequence sampling method. Mechanistic models include input uncertainties that lead to deviations in model estimations. Both time-dependent and independent global sensitivity of moisture, sample temperature, sample's internal pressure, their spatial homogeneity, and drying time were assessed using Lasso regression (a variable selection method that penalises the coefficients using $l_1$ norm). The stochastic results of the mechanistic investigation showed that the effects of the input variables are almost identical both as static and time-dependent variables. Lasso regression results indicated that operational and model uncertainties cause varying changes in the magnitude and direction of the stochastic model predictions throughout the process. By contrast, the homogeneity properties of the dry product are not caused by these variations and heterogeneous distribution of the electric field. Additionally, electrical conductivity, oven temperature, applied voltage, and initial moisture were found to be the variables which have the most significant effect on all the variables which were examined in terms of operational and model uncertainties. *Practical Applications.* The present study investigates the stochastic behaviour of the OAD system through the mechanistic model and using a probabilistic modelling approach. To the best of our knowledge, in addition to being the first study to probabilistically evaluate the OAD system, we are introducing Buzas and Gibson's evenness value for the first time in the food science/technology literature. This measure serves as a numerical indicator of the spatial distribution homogeneity of the physical properties of the sample. The study's findings and proposed methodologies will have further applications not only for researchers but also for manufacturers, particularly for those involved in the design and analysis of new drying and food systems in general. Moreover, the presented methods and novel homogeneity measures are generic tools; they can be easily adapted to other process improvement practices involving input/output uncertainty/variability.

## 1. Introduction

Drying, especially convection and drying under the sun, is one of the well-known methods of prolonging the shelf life of foods. However, these popular drying methods have some disadvantages such as high amount of energy consumption and extensive loss of quality and nutrients, climate dependency, and chemical and/or biological contamination threats

[1–7]. To address these issues, researchers generally prioritise the development of alternative and energy- and time-efficient technologies [8–11].

One of these technologies is ohmic-assisted convective drying (OAD) which was—to our knowledge—first introduced in the literature with our previous study [12]. In this study, a mechanistic model for OAD that consist of momentum, heat, and mass transport, as well as ohmic heating, was established. Furthermore, parametric optimisation of process conditions and changes in product quality as a function of their variations (voltage, air temperature, and velocity) have recently been studied [13]. In each of these studies, empirical and mechanistic modelling methods were used based on a top-down modelling approach in which the major underlying drying mechanisms were characterised without in-depth analysis [14]. However, modelling a food drying system is a complicated and challenging task since there are many factors influencing a performance drying system, including drying temperature, airflow rate, sample qualities, and pretreatment [3]. Since the variations of the input parameters such as material properties, as well as the model parameters, might have different and complicated behaviours, the developed model cannot be implemented for other materials/systems [15]. As a result, it is vital to address the effects of uncertainty sources in the analysis and design process of systems of interest to assist in building an effective approach preventing deviations from the expected performance [16]. That is why there are a large number of examples of probabilistic evaluation of food models/systems [17–21]. To the best of our knowledge, no study has yet been presented on the probabilistic evaluation of the OAD in response to uncertainty of model parameters to explain stochastic system behaviours and investigate the underlying mechanisms in depth.

The instability of a model prediction can arise from *model* and *operational uncertainties* which are also called (i) *structural uncertainty* and (ii) *parameter uncertainty*, respectively [22]. Structural uncertainties are frequently associated with physics assumptions in the mechanistic model, whereas parameter uncertainties arise from variances in the input parameters, which can have a significant impact on simulation estimates but cannot be known precisely due to natural variations in food materials. On the other hand, sensitivity analysis can be performed using two general methods, which are (i) *local* and (ii) *global* sensitivity analyses. Global sensitivity analysis provides a better understanding but is often more complex and requires more computational effort [23]. One of the most usually recommended and used methods to imitate input uncertainty and emphasize a system's global sensitivity is Monte Carlo (MC) simulation [24, 25]. Although the MC method has been previously used for probabilistic evaluation of the systems, including food drying [26–29], the present study is the first example of its implementation for OAD system.

Another critical issue required to consider is the heating uniformity of ohmic heating systems. The homogeneous treatment of food materials using ohmic heating is an important and challenging issue, especially in foods with spatial inhomogeneities in electrical conductivity. As a result, heterogeneous moisture and temperature distribution can cause local over- or underprocessing problems [30] or the formation of soggy surfaces [31], reducing product quality and system production efficiency. Although no soggy surfaces were observed at the end of drying in our preliminary study, heterogeneous heating (due to spatial variations in moisture and electrolyte concentration in samples) and overshoots (around electrodes) were clearly visible (please see Figure S1 in Supplementary Materials) [12]. Therefore, a thorough understanding is required to improve the OAD design and performance for further studies. To accomplish this, rather than the commonly used visual inspection that allows for subjective evaluation, Buzas and Gibson's evenness value ($E$) [32] was adapted and used in the present study for the first time in the food-related literature, as far as we know. It was used for both dynamic (time-dependent) and static (end-of-drying) analyses of spatial homogeneity of model predictions, along with uncertainty analysis.

Therefore, the current study is aimed at (i) assessing the probabilistic behaviour of the OAD against the combined impact of operational and model uncertainties, (ii) identifying model variables with the greatest impact on the stochastic model predictions, (iii) introducing the adapted use of Buzas and Gibson's evenness value as a numerical measure of static and dynamic model homogeneity, and (iv) drawing a perspective for future efforts regarding possible improvement of the OAD system.

## 2. Methodology

*2.1. OAD Equipment and Numerical Method.* The OAD system consists of a tunnel-type hot air dryer (Eraktek Innovation, Konya, Türkiye) equipped with custom-built lab-scale electrode apparatus (ohmic cell with 6 needle-type electrodes, each with a 3 mm diameter) and an AC power supply (max operation conditions are 400 V-10A AC at 50–60 Hz) (Eraktek Innovation, Konya, Türkiye). A schematic representation of the OAD system is given in Figure 1.

The mechanistic model was developed for the drying of potato slices (rectangular prisms, $40 \times 40 \times 5$ mm) using OAD system under different process conditions (air velocity: 0.74, 1.55, and 2.15 m/s; air temperature: 50 and 60°C; and voltage: 75, 100, and 125 V without interruption during drying) until the desired moisture content ($m_{db} = 0.1$) was attained. The model of OAD system employs coupled heat and mass transport, as shown in Figure 2:

(i) Convective heat and mass transfer between the potato surfaces and the hot drying air surrounding them

(ii) Heat generation by electric current

(iii) Internal heat transfer by conduction and convection

(iv) Internal mass transfer by diffusion and convection

(v) Evaporation/condensation of water in different internal locations and on the surfaces

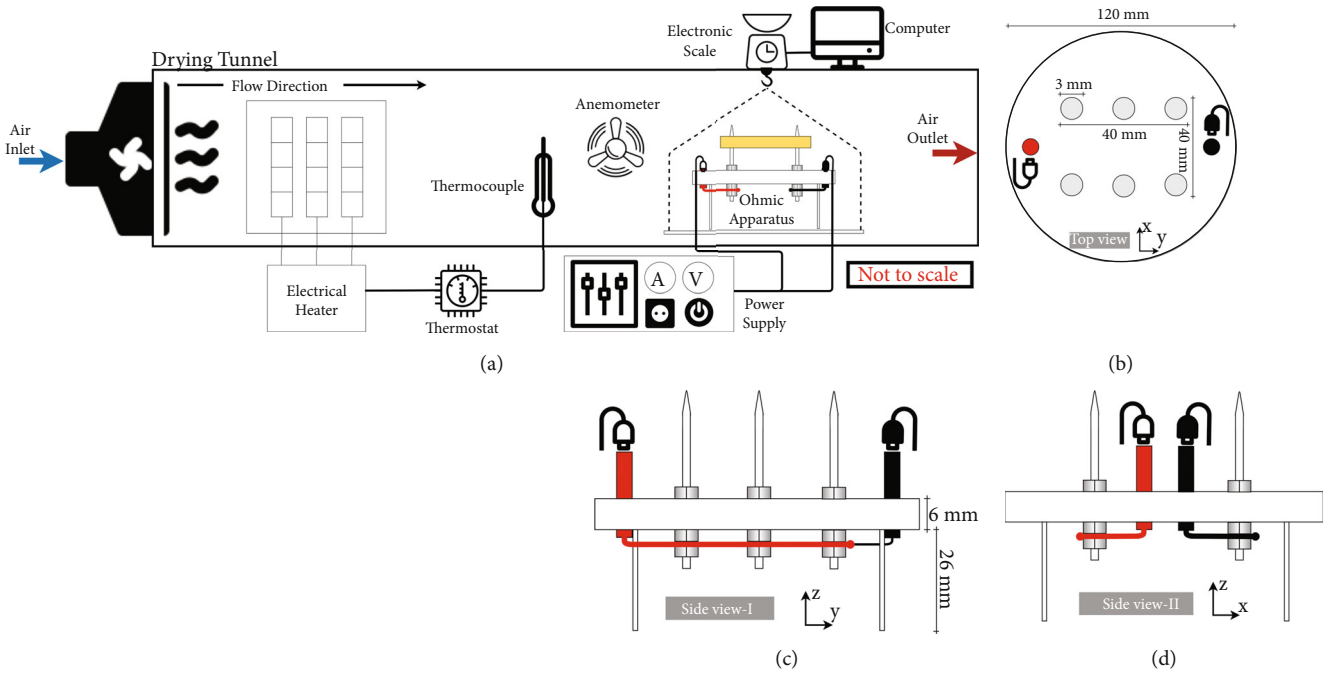


FIGURE 1: Schematic illustration of (a) the drying tunnel and the ohmic heating apparatus from (b) top view (c) and (d) side views where red and black lines are phase/neutral power supply cables, respectively (reused material from Innovative Food Science & Emerging Technologies, A novel drying system - simultaneous use of ohmic heating with convectional air drying: System design and detailed examination using CFD, 72, 102727, Turgut et al. [12], Copyright Elsevier (2021)).

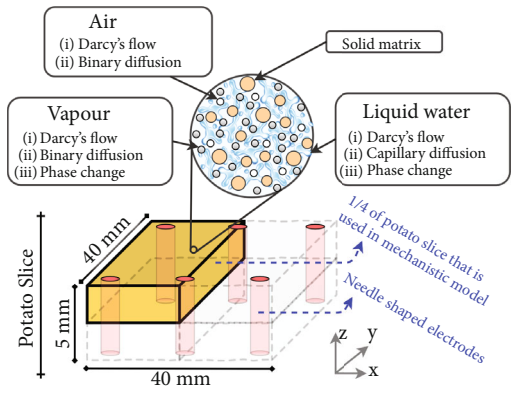


FIGURE 2: Schematic illustration of transport mechanisms for different phases and the computational domain for the drying simulations.

A summary of the governing equations of the mathematical model and the list of uncertain input parameters can be found in Tables 1 and 2. More information about the OAD equipment, experimental model validation studies, and mechanistic model details (such as the assumptions, input parameters, calculation of the transfer coefficients, and solution strategies) can be found in Turgut et al. [12]. Moreover, a brief list of assumptions, input parameters, symbols, values, and corresponding units is given in Supplementary Materials (please see Table S1).

*2.2. Probabilistic Evaluation Setup.* To evaluate the probabilistic behaviour of the OAD system, MC simulations are done in three steps: (1) modelling a system of interest as a sequence of probability distribution functions, (2) repeated sampling from a specified random selection until convergence, and (3) calculating the relevant statistics [25]. Figure 3 shows a schematic description of uncertainty assessment.

*Step 1.* The first step in running an MC simulation is to determine the uncertainty of each model input parameter. To determine the uncertainty range of the input parameters, expert opinion (opinion based on our experimental observations), experimental data, and/or literature data may all be used. For example, the range for the initial moisture content ($m_{db0}$) was obtained from measured experimental data (marked with • in Table 2). Based on literature and experimental observations, the uncertainties of other input parameters were classified as low (*), medium (**), and high (***) indicating 15%, 30%, and 50% of variability around the nominal value, respectively. For the operating parameters (oven temperature ($T_{oven}$), air velocity ($u_0$), and applied voltage ($V$)), a 15% variability around the nominal values was considered, based on the experimental observations and the limits of the experimental OAD setup. Furthermore, the diffusion coefficient of gases ($D_{eff,g}$) and the multipliers for electrical conductivity and capillary diffusivity ($k_\sigma$ and $k_w$) were sampled within a range of medium variability (30%). Finally, the uncertainty of the evaporation rate constant ($K$) was set to high variability (50%) because the values reported in the literature widely range from 1 to 1000 for different food processes [33–37].

Table 1: Summary of physics equations of the model ohmic heating-assisted convection drying system [12].

Mass and momentum transfer

GE:

$$\begin{cases} (\partial c_i/\partial t)+\nabla\bullet(-D_i\bullet\nabla c_i + u_i\bullet c_i) = \pm R_i \\ u_i = \left(-\kappa_{(\mathrm{in},i)}\bullet\kappa_{(r,i)}\right)\nabla P/(\phi S_i \mu_i) \longrightarrow \begin{cases} u_{\mathrm{eff},w} = u_{\mathrm{w}} + D_{\mathrm{cap}}\nabla c_w \\ u_{\mathrm{eff,g}} = u_{\mathrm{g}} + D_{\mathrm{eff,g}}\nabla c_{\mathrm{g}} \end{cases} \end{cases}$$

BC:

$$\begin{cases} P_{\mathrm{sur}} = P_{\mathrm{amb}} \\ n_{v,\mathrm{sur}} = c_v u_{n,v} + h_m \phi S_{\mathrm{g}}(c_v - c_{v,\mathrm{oven}}) \\ n_{w,\mathrm{sur}} = h_m \phi S_w (c_v - c_{v,\mathrm{oven}}) + (c_w u_{n,w})\big|_{S_w=1} \end{cases}$$

Heat transfer and electric physics

GE:

$$\begin{cases} \rho_{\mathrm{eff}} c_{p,\mathrm{eff}}(\partial T/\partial t)+\nabla\bullet\left(-k_{\mathrm{eff}}\bullet\nabla T + \rho_{\mathrm{eff}} c_{p,\mathrm{eff}} u_{\mathrm{eff}}\bullet T\right) = \pm R_i M_w L + Q \\ Q = \eta\sigma|\nabla \mathrm{V}|^2 \\ \nabla\bullet\sigma\nabla \mathrm{V} = 0 \end{cases}$$

BC:

$$\begin{cases} q_{\mathrm{sur}} = h_T(T - T_{\mathrm{oven}}) - n_{v,\mathrm{sur}} M_w c_{p,v} T \\ -h_m \phi S_w M_w (c_v - c_{v,\mathrm{oven}})\left(\lambda + c_{p,v} T\right) \\ -(c_w u_{n,w}) M_w c_{p,v} T\big|_{S_w=1} \\ \mathrm{V} = \begin{cases} 0, & @\mathrm{ground} \\ 100, & @\mathrm{electric\ source} \end{cases} \\ \nabla \mathrm{V} = 0 @ \mathrm{boundaries\ except\ electrodes} \end{cases}$$

Thermophysical and physical properties and constitutive equations

$$\begin{cases} a_w = \exp\left(-0.033/m_{\mathrm{db}}^{1.497}\right) \\ P_{v,\mathrm{sat}} = \exp\left[-580.2206/T + 1.3915 - 0.0486T + 0.4176\times10^{-4}T^2 - 0.01445\times10^{-7}T^3 + 6.546\ln(T)\right] \\ m_{\mathrm{db}} = (c_w M_w)/[(1-\phi)\rho_s] \\ P = p_a + p_v \\ \rho_{\mathrm{eff}} = \phi\left(S_g\rho_g + S_w\rho_w\right) + (1-\phi)\rho_s \\ c_{p,\mathrm{eff}} = x_g\left(\omega_v c_{p,v} + \omega_a c_{p,a}\right) + x_w c_{p,w} + x_s c_{p,s} \\ k_{\mathrm{eff}} = \phi\left[S_g(\omega_v k_v + \omega_a k_a) + S_w k_w\right] + (1-\phi)k_s \\ \rho_i = (p_i M_i)/(RT) \\ c_{v,\mathrm{oven}} = \left(\mathrm{RH\%}_{\mathrm{oven}}\, P_{\mathrm{sat}}\big|_{T_{\mathrm{oven}}}\right)/(R\, T_{\mathrm{oven}}) \\ \sigma = 0.25(1 + 0.030(T - 298.15)) \\ \eta = \begin{cases} [(m_{\mathrm{db}} - m_{\mathrm{db,lim}})/(m_{\mathrm{db0}} - m_{\mathrm{db,lim}})]^3, & m_{\mathrm{db}} > m_{\mathrm{db,lim}} \\ 0, & m_{\mathrm{db}} \le m_{\mathrm{db,lim}} \end{cases} \\ D_{\mathrm{cap}} = 1\times10^{-8}\mathrm{e}^{(-2.8+2m_{\mathrm{db}})} \end{cases}$$

(i) GE: governing equations; BC: boundary conditions. (ii) For the definitions of the abbreviations and symbols given in the table, please see Nomenclature. (iii) For the full list of BCs and initial conditions and details of GEs, please see Turgut et al. [12]. Moreover, a brief list of assumptions, input parameters, symbols, values, and corresponding units is given in Supplementary Materials (please see Table S1).

*Step 2.* The Halton sequence (HS) sampling method was used to reproduce the uncertainty of the input parameters, because HS was previously described as a rapid converging sampling method for MC simulations compared to other sampling techniques [18]. Detailed information about HS can be found in the study by Kroese et al. [38]. In total, 1000 randomly paired samples were chosen, each ($\theta_i$) with one value for every unknown input parameter.

$$\theta_i = [\theta_{1i}, \theta_{2i}, \theta_{3i} \cdots, \theta_{mi}], \text{ for } i = 1, 2 \cdots n, \quad (1)$$

where $n$ corresponds to the input parameter number (9) and $m$ is the number of reproduced input levels for each uncertain variable using HS (1000). To test the convergence of the MC simulation, the sample size ($m$) in the current study was increased from 25 to 1000 until it no longer influenced the sensitivity analysis results.

*Step 3.* The simulations were conducted using randomised input space, which included $m \times n$ different combinations of input variables. For every combination of inputs ($\theta_i$), one simulation was run. In the end, solution matrices consisting of the volume averages of $m_{\mathrm{db}}$, $T$, and $P$ as a function of time (1 min intervals between 0 and 300 min) for $m \times n$ combinations were obtained. In addition, homogeneity for the distribution of each value ($E_{m_{\mathrm{db}}}$, $E_T$, and $E_P$) was calculated as a function of time. The drying time (DT) of the

Table 2: Uncertainty ranges for input parameters.

| Parameter | Unit | Nominal value | Range Min–max | Source |
|---|---|---|---|---|
| Initial moisture content ($m_{db0}$)$^{\bullet}$ | g water g$^{-1}$ dry mater | 4.78 | 2.72-6.84 | [a] |
| Air velocity ($u_0$)$^{*}$ | m s$^{-1}$ | 1.5 | 1.275-1.725 | [b] |
| Drying temperature ($T_{oven}$)$^{*}$ | °C | 60 | 51-69 | [b] |
| Voltage ($V$)$^{*}$ | V | 100 | 85-115 | [b] |
| Evaporation rate constant ($K$)$^{***}$ | s$^{-1}$ | 10 | 5-15 | [b] |
| Limiting moisture content for electrical conductivity ($m_{db,lim}$)$^{\bullet}$ | g water g$^{-1}$ dry mater | 0.26 | 0.15-0.37 | Calculated from [c] and [d] |
| Diffusion coefficient of gases ($D_{eff,g}$)$^{**}$ | m$^2$ s$^{-1}$ | $2.6 \times 10^{-6}$ | $(1.82 - 3.38) \times 10^{-6}$ | [e] |
| Multiplier for $\sigma$ ($k_\sigma$)$^{!,**}$ | — | 1 | 0.7-1.3 | [b] |
| Multiplier for $D_{cap}$ ($k_w$)$^{!,**}$ | — | 1 | 0.7-1.3 | [b] |

$^{\bullet}$Obtained from measurement. $^{*}$±15% of the nominal value. $^{**}$±30% of the nominal value. $^{***}$±50% of the nominal value. $^{!}$The $k_\sigma$ and $k_w$ are multipliers for electrical conductivity ($\sigma$, S m$^{-1}$) and capillary diffusivity ($D_{cap}$, m$^2$ s$^{-1}$) calculated from the corresponding equations of $\sigma$ and $D_{cap}$ given in Table 1. [a]Experimental. [b]Present study. [c]Lewicki [55]. [d]Kaymak-Ertekin and Gedik [56]. [e] Halder et al. [36].

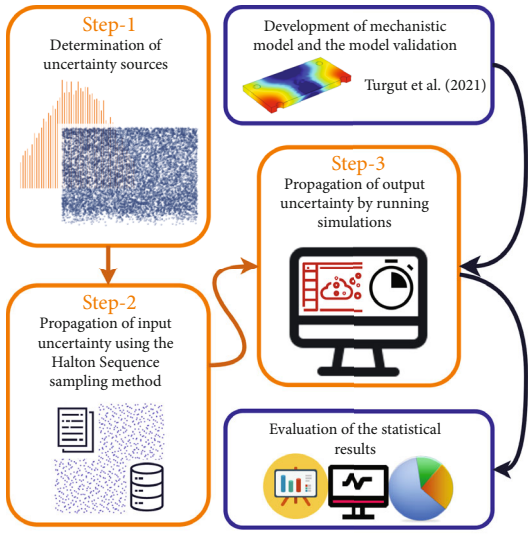


Figure 3: Schematic representation of the uncertainty evaluation with Monte Carlo procedure.

potato samples (an important output of the drying process model) was measured from the beginning of the process until the time when $m_{db} = 0.1$. DT was analysed to evaluate the effect of input uncertainties on the performance of the OAD system. Moreover, the final $E_{m_{db}}$, $E_T$, and $E_P$ values of the samples at the end of drying (corresponding to the homogeneity values at $t = DT$) were evaluated as scalar model outputs. The means and percentiles of 10% and 90% of the model predictions were used to illustrate the distribution of the results.

*2.3. Statistical Evaluation of the Stochastic Model Predictions.* To assess the sensitivity/uncertainty of the parameters, the Lasso regression (LR) method was used. LR works in principle like multiple linear regression (MLR), but with an additional penalty term for the sum of squared residuals (RSS) [39]. MLR models have the following general equation form.

$$\hat{y} = b_0 + \sum_{i=1}^{n} b_i x_i, \tag{2}$$

where $\hat{y}$ is the model prediction, $b_0$ is the intercept term, $b_i$ is the corresponding model coefficient, and $x_i$ describes each input parameter. The least squares optimisation was used to determine model coefficients ($b_i$) by minimising the RSS.

$$\text{RSS} = \sum_{j=1}^{m} \left( y_j - \left( \sum_{i=1}^{n} b_0 + b_i x_i \right) \right)^2. \tag{3}$$

The MLR models have a low bias but a high variance while having a high coefficient of determination. This means that a minor change in the training data might result in a significant change in the model parameters. Thus, ordinary least squares minimisation does not yield the optimal subset of them. Therefore, various regularisation methods (such as ridge and Lasso regressions) can be used to find the optimal subset of model parameters that play with the variance-bias trade-off. Although the theoretical backgrounds of ridge and Lasso are similar, LR is advantageous when the model parameter values are extremely small (close to 0) due to the use of the $l_1$ norm as the shrinkage term [39]. The addition of a hyperparameter ($\lambda$) with a shrinkage penalty to the minimisation term ($MT$) takes the following form for LR [40].

$$\text{MT} = \text{RSS} + \lambda \sum_{i=1}^{n} |b_i|. \tag{4}$$

The $\lambda$ hyperparameter controls the degree of fit of the predictive model. At a value of $\lambda \longrightarrow 0$, the prediction

model approaches MLR (with lower model bias and higher variance). As the value increases, the model variance of LR decreases and the model bias increases. As a result, the coefficients of the model parameters shrink towards zero and all model coefficients become equal to zero with $\lambda \longrightarrow \infty$ [39, 40]. However, under the same conditions, none of the model coefficients are equal to 0 when ridge regression is used. Because of these properties, LR provides a simpler model and can be used as a feature selection/ranking method [39].

In this case, before implementing LR as a ranking method, all model variables were transformed into the standard normal distribution. Then, LR was repeated for an array of $\lambda$ values, starting from 0.01 and increasing to 1. In this way, standardised model coefficients (SMC) were calculated for a series of $\lambda$ values. To assess the sensitivity of the scalar model outputs to uncertainty input variables, the SMC results were used in comparison to the $\lambda$ values. To evaluate time-dependent output variables, the same procedure was repeated for each minute of the drying process and the minimum $\lambda$ values where the model coefficients were zero ($\lambda_i|_{b_i=0}$) were extracted and plotted against time.

*2.4. Spatial Homogeneity.* For product quality, homogeneity of sample properties is an important parameter for food processing systems based on ohmic heating. However, homogeneity is usually assessed visually by looking at model results, e.g., the coloured plots of a model (such as 2D surface, 3D volume, or contour plots), which can be subjective. Buzas and Gibson's evenness value ($E$) can be used to overcome this [32]. Therefore, we used $E$ to assess the homogeneity of the model behaviour with respect to the spatial distribution of the variables $m_{\mathrm{db}}$, $T$, and $P$. With this method, it is possible to make a numerical and objective inference about the homogeneity of the variables. To find $E$, we first extracted the required output variables from the nodes of the mesh for each minute of drying and then calculated the Shannon-Wiener diversity indices ($H$) (Eq. (5)) [32, 41]. $H$ is a well-known $\alpha$-diversity index used to determine the homogeneity of the distribution of a value over an area/domain [41]. In our case, this domain is the volume of the potato slice in the mechanistic model and $m_{\mathrm{db}}$, $T$, and $P$ are the output variables to be evaluated.

$$H = -\sum_{i=1}^{N} p_i \ln(p_i), \tag{5}$$

where $p_i$ is the proportional value of each extracted output variable ($c_i$) in a one-minute time interval (Eq. (6)) and $N$ is the number of total observations for the given output per minute.

$$p_i = \frac{c_i}{\sum_{i=1}^{N} c_i}. \tag{6}$$

To determine $c_i$, being output variables ($m_{\mathrm{db}}$, $T$, and $P$), the time-dependent data were divided into bins of sizes 0.01, 0.5, and 0.05 and the number of observations falling into each bin was counted. To calculate $p_i$, this number was divided by the total number of observations. Although the $H$ value is a good indicator of the spatial homogeneity of the data, it can be further improved by normalisation. This gives us the Buzas and Gibson's evenness value ($E$) [32].

$$E = \frac{e^H}{N}. \tag{7}$$

After the transformation according to Eq. (7), $E$ values range between 0 and 1. If the spatial distribution of the variable of the interest is completely homogeneous, then $E$ takes the value of "1," and if the homogeneity decreases, the $E$ value decreases close to "0," indicating high heterogeneity.

*2.5. Model Implementation and Solution.* Propagation of input uncertainties with HS was performed using MATLAB® (version 2016b). The model equations (Table 1) for different combinations of inputs were solved using COMSOL Multiphysics® LiveLink™ for MATLAB (version 5.3a, Burlington, USA) (for more details, please see Turgut et al. [12]). The data extraction and the calculation of the sensitivity indices were made using the COMSOL-MATLAB environment. The statistical calculations of the extracted data were completed using Python language (version 3.7). Array/matrix and data manipulation/analysis operations were done using the "NumPy" and "pandas" libraries, while statistical and machine learning tasks were carried out using the "scikit-learn" and "SciPy" libraries. "Plotly" library was used to create graphical objects.

## 3. Results and Discussion

*3.1. Model Outputs and Uncertainty of Model Predictions.* Figure 4 shows the mean and the 10$^{\mathrm{th}}$ and 90$^{\mathrm{th}}$ percentiles of $m_{\mathrm{db}}$, $T$, and $P$ resulting from the $N = 1000$ simulation (for a detailed description, see Section 3.2). With the help of Figure 4, one can see how the output variables are distributed depending on the uncertainty of the input parameters as drying time progresses. The uncertainty range increases for $m_{\mathrm{db}}$ and $T$ with drying time, whereas it remains nearly constant for $P$ over the entire drying time. For $m_{\mathrm{db}}$, the same behaviour is seen when ohmic heating begins to weaken. In addition, the uncertainty of $T$ grows steadily until the completion of the drying process (Figures 4(a) and 4(b)). Except for the period when ohmic heating is active, there is no clear uncertainty for $P$ compared to $m_{\mathrm{db}}$ and $T$ (Figure 4(c)).

In general, Figure 4(a) can be examined by dividing it into two parts. The first part lasts up to 20 minutes and has higher slopes (indicating a higher drying rate due to ohmic heating of the sample) than the rest of the drying. This region was previously referred to as the "accelerated drying step" because of higher drying rates when compared to the rest of the process [12]. The accelerated drying step approximately involves the combination of *heating*, *streaming,* and *enthalpic* periods of drying [42]. Different mechanisms can occur, altering the effectiveness of ohmic heating on the increased drying rate. One of these possible mechanisms is the modifications in potato structure, also named

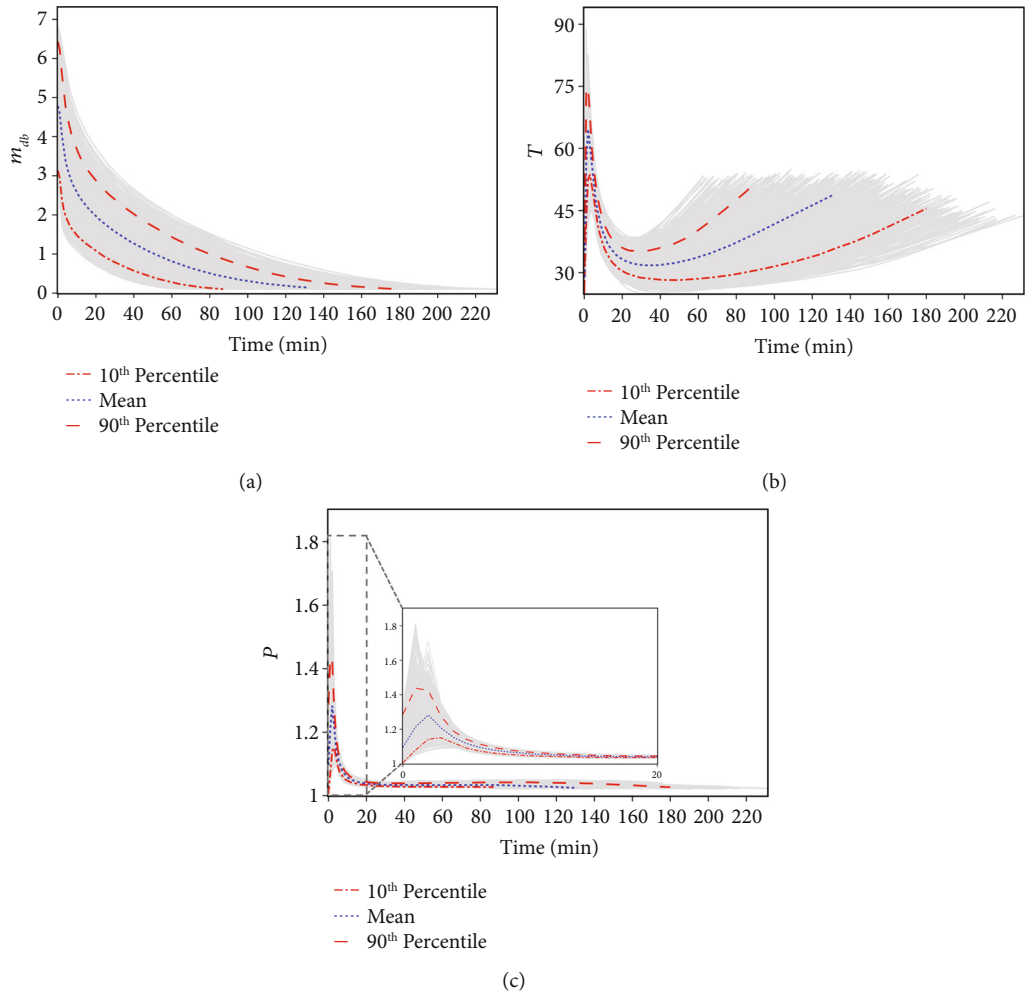


Figure 4: Uncertainty of volume averages for (a) moisture content ($m_{db}$, g water/g dry matter), (b) temperature ($T$, ˚C), and (c) pressure ($P$, atm) using mean and 10th and 90th percentiles (the 1000 Monte Carlo simulations are shown in grey spaghetti plots).

"tissue damage," as a result of electroporation, which occurs even at very low electric fields (≥20 V cm$^{-1}$) [43, 44]. During processing, this tissue damage promotes the release of water from the cell wall, enhances the transport of water molecules, and increases the drying rate. It was previously discovered that changes in porosity, density, and textural characteristics of samples after ohmic heating (as a pretreatment) increase drying performance [44–47]. These structural changes are linked to increased water diffusivity through the tissue [43]. However, in our scenario (simultaneous use of ohmic heating and convection), it was thought that the very quick temperature increase in the drying material, rather than structural changes in the potato tissue, was the major contributing factor to rapid drying with OAD. As shown in Figures 4(b) and 4(c), the temperature of the entire domain rises too quickly due to volumetric heating (as for microwave [31]) in the ohmic heating-dominated zone of the drying. Therefore, the average $T$ of the samples reached the maximum rapidly, which was approximately between 45 and 90˚C for 1000 simulations of MC. There is no doubt that the maximum temperatures (even higher temperatures than seen in Figure 4(b) since average $T$ is given with it) would be expected primarily in the regions near the electrodes. It has been reported that when volumetric heating methods are used, the temperature rises above the boiling point of water [31]. For example, microwave drying can generate temperatures higher than 150˚C for porous materials [42]. As previously discussed in our earlier study [12], the reason for temperatures above the boiling point of water at 1 atm (100˚C) is the internal pressures of the potato exceeding the atmospheric level. Figure 4(c) shows that the maximum average $P$ of the potato slice was between 1.1 and 1.8 atm confirming our previous argument. However, reciprocally, the reason for the overpressures during OAD is the increased evaporation at high temperatures caused by ohmic heating. Furthermore, the much higher temperatures in the region of interest are related to the high evaporation rates, which cause overpressures. As a result, the temperature and pressure in the domain mutually rise and trigger each other until the temperature of the liquid water falls to a level that mitigates the effects of ohmic heating. Similarly, high pressure values (up to 4 atm gauge pressure) for combined microwave convection drying of softwood materials have already been recorded [42]. And smaller

overpressures have also been observed during microwave drying for food [31, 48, 49].

Following the accelerated drying step, OAD moves on to the "regular drying step" [12]. This drying step begins when the sample's temperature falls to a level close to its initial level, and the process then has characteristics similar to conventional drying. During this step, the air velocity and air temperature are the main factors affecting the drying characteristics [50]. The drying rate decreases towards the end of the OAD process as the removable moisture content in the sample domain decreases continuously during the regular drying step. Moreover, with the end of the accelerated drying step, the overall $P$ of the domain decreases to atmospheric pressure and follows a stable trend until the drying process is completed. Therefore, only a few barely perceptible increases in $P$ can be seen in Figure 4(c), which are most likely from simulations with higher air temperatures. Despite $P$, the samples' average $T$ begins with a slight increase at regular drying steps. Because the surface temperature is lower than the ambient temperature ($T_{\text{oven}}$), there is an intense flow of energy from the drying air to the sample. The evaporation rate and energy spent on it decrease between 20 and 40 minutes of drying due to the reduced moisture content and low drying rate. As a result, the majority of the energy gained by convection begins to be spent on raising the temperature of the sample surfaces. Then, as the water content decreases over time, a considerable amount of the energy is used to raise the temperature of the sample [12, 51]. As a result, as the OAD process nears completion, the temperature of the sample approaches the ambient temperature.

Homogeneity of sample properties, such as moisture and/or temperature homogeneity, is an important parameter for ohmic heating-based food processing systems. This is because variations in the electric field can cause problems with quality and production efficiency. For example, these differences can cause local over- or underprocessing issues in various regions of the sample [30]. Furthermore, soggy surfaces may appear as a result of moisture accumulation in some parts of the material [31]. So, to analyse the effect of OAD on them, time-dependent spatial homogeneity variations for the output variables ($E_{m_{\text{db}}}$, $E_T$, and $E_P$ for $m_{\text{db}}$, $T$, and $P$, respectively) were computed and illustrated in Figure 5. The figure shows that at the beginning of the OAD process, all homogeneity values are equal to 1. This means that the output variables in the sample volume are at first completely homogeneous. This is because the initial values are the same everywhere and are equal to the model's set values. With the start of the OAD process, the ohmic heating is promptly initialised and the sample domain begins to heat up, resulting in hot and cold regions where the ohmic heating is effective and ineffective, respectively. This leads to a decrease in the $E_T$ value, which indicates a decrease in the spatial homogeneity of $T$, or in other words an increase in spatial variations/heterogeneity. This also affects the moisture and pressure distributions across the sample domain, and $E_{m_{\text{db}}}$ and $E_P$ show a similar trend to $E_T$. $E_{m_{\text{db}}}$ reaches low values between 0.45 and 0.75 before $E_T$ and $E_P$ due to the rapid evaporation of liquid water in the domain. However, after the accelerated drying step is completed, the homogeneity of the variables begins to increase. $E_T$ and $E_P$ reach relative stability by the end of the drying process. This is due to $T$ and $P$ approaching the environment values and the process gradually reaching equilibrium for these variables. $E_{m_{\text{db}}}$, on the other hand, shows a slight decrease and may be attributed to the difference in $m_{\text{db}}$ values between the inner and outer portions of the sample.

The heterogeneous distribution of sample properties (such as temperature and moisture) causes undesirable changes during the process as previously discussed by Turgut et al. [12]. For instance, overshoot regions can be observed depending on the applied electrical potential, due to rapid water removal and a decrease in electrical conductivity caused by the sudden temperature increase. These changes, combined with the rapid drying of the inner areas (the region between the electrodes), result in a decrease in electrical conductivity and it leads to an interruption of the electrical field. Thereby, not only does the ohmic heating efficiency decrease, but burnt areas of the sample near the electrode surfaces are also observed. Furthermore, the heterogeneous temperature distribution increases heterogeneous evaporation/pressure and moisture movement from the interior to the exterior of the domain. Finally, depending on the applied voltage, this resulted in an accumulation of excess moisture at the sample boundaries, which can cause slightly soggy surfaces typical of volumetric drying processes (similar phenomena occur with microwave heating) [31].

*3.2. The Use of Lasso Regression for Global Uncertainty Analysis.* The LR method was used to compare the effects of uncertain input parameters on the model's output variables. For time-dependent model outputs (that are volume averages of $m_{\text{db}}$, $T$, and $P$), $\lambda|_{b_i=0}$ (the $\lambda$ values that make the LR coefficients equal to zero) was used as a function of time. On the other hand, SMC against $\lambda$ was presented for scalar variables (DT and final values of $E_{m_{\text{db}}}$, $E_T$, and $E_P$). However, as the first step, the effect of sample size ($N$) on SMC was evaluated to conclude the convergence of the MC simulation. The effect of sample size on SMC vs. $\lambda$ is depicted in Figure 6 for this purpose. For clarity, only the results for $m_{\text{db}}$, $T_{\text{oven}}$, and $V$ were given. The high deviation for $m_{\text{db}}$ is easily seen in Figures 6(a)–6(c) for small sample sizes, i.e., 25-200. Increasing $N$ (for $N > 200$) had no discernible effect on $\lambda|_{b_i=0}$ regarding $V$. However, with increasing sample size, $\lambda|_{b_i=0}$ of $m_{\text{db}}$ and $T_{\text{oven}}$ reached a nearly constant value after 750-1000 simulations. As a result, all further analyses in the rest of the paper are performed for $N = 1000$.

Figure 7 shows the SMC values of the predictive LR models at various $\lambda$ values for DT and $E_{m_{\text{db}}}$, $E_T$, and $E_P$ at the end of the drying process (simulations were stopped when the volume average of $m_{\text{db}} \leq 0.1$). As for LR, the SMCs of model parameters tend to approach zero as $\lambda$ increases. It is worth noting that the parameters that reach $\lambda|_{b_i=0}$ earlier have weaker effects on the model outputs than on other explanatory variables and vice versa. Thus, the values of $\lambda|_{b_i=0}$ can be used as a direct index showing the relative

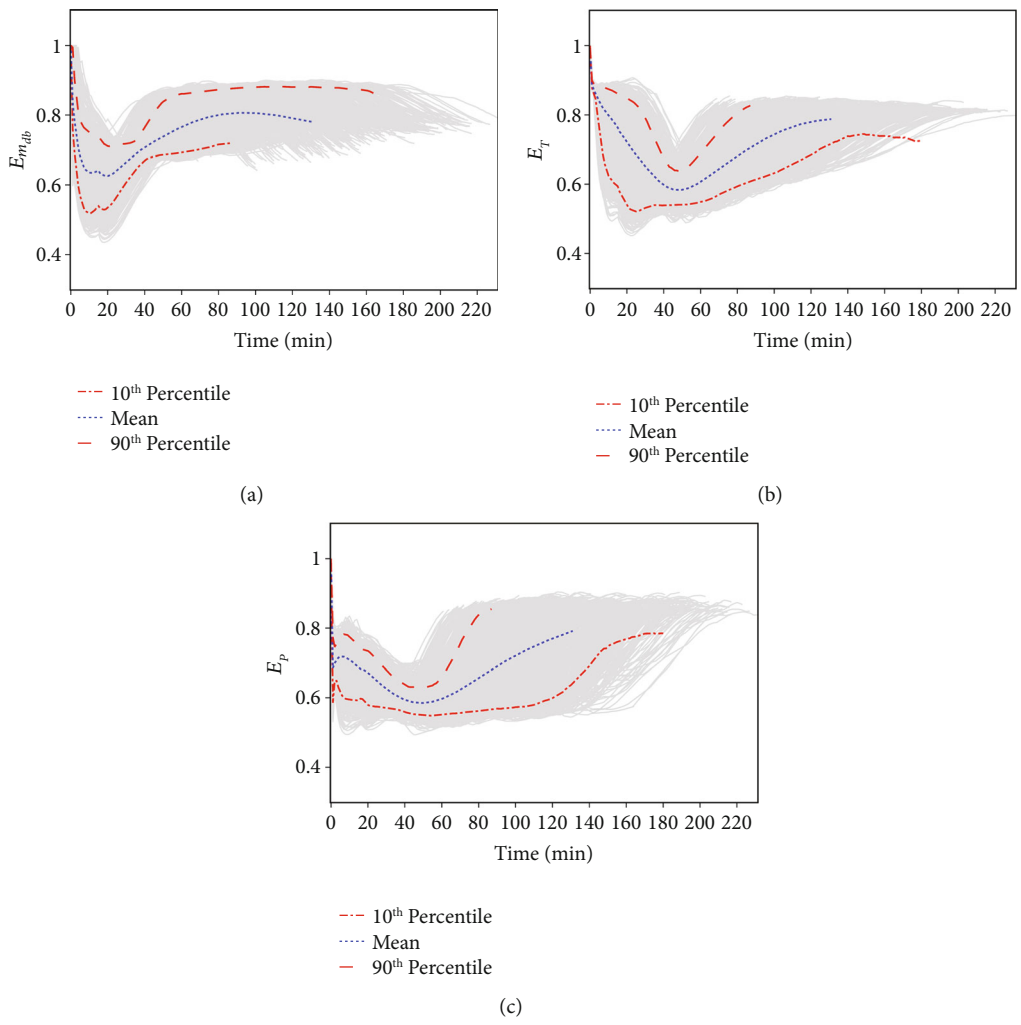


FIGURE 5: Uncertainty of volumetric averages of Buzas and Gibson's evenness values for (a) dry basis moisture content ($E_{m_{db}}$), (b) temperature ($E_T$), and (c) pressure ($E_P$) using mean and 10th and 90th percentiles (the 1000 Monte Carlo simulations are shown in grey spaghetti plots).

influence of the input parameters on the stochastic outputs. Furthermore, the sign of SMC values indicates whether the correlation between input and output variables is positive or negative.

Figure 7(a) illustrates the effects of the input parameters on the predictions of DT. DT was previously defined as the amount of time required to reduce the dry basis moisture content of the potato slice to 0.1. According to the results, the most effective model parameters on DT are, in decreasing order, $m_{\mathrm{db0}}$, $T_{\mathrm{oven}}$, $K$. With nearly equal efficiency, these parameters are followed by $k_\sigma$ and $V$. Other input variables either have very little effect, e.g., $D_{\mathrm{eff,g}}$ and $k_w$, or no impact as $m_{\mathrm{db,lim}}$ has. Only $m_{\mathrm{db0}}$ has a positive correlation indicating that a higher initial moisture content causes a higher DT as expected. Apart from the effect of $m_{\mathrm{db0}}$, $k_\sigma$ and $V$ were found to have smaller effects on DT than $T_{\mathrm{oven}}$ because ohmic heating directly affects the physical properties of the material (temperature, pressure) during a limited period of OAD (see Section 3.3 for a detailed explanation). However, in addition to their direct effects, $k_\sigma$ and $V$ also have some real-world influences on other material properties (such as structural deformation and increase in diffusion coefficient). As a result of these modifications, ohmic heating has an indirect positive impact during the regular drying period, as observed in our experimental study [13]. Since air velocity and temperature are important parameters for convection drying systems [50], $T_{\mathrm{oven}}$ (as an important parameter affecting heat and mass transfer coefficients) has a significant influence on DT during the *regular drying step*. The evaporation rate constant ($K$) is a parameter that indicates the evaporation rate and has a dimension of reciprocal time in which phase change takes place [36]. $K$ can have various values depending on the process and material [33–37]. Therefore, it is a critical term for defining the phase change rate of water and has a considerable impact on the DT of an OAD system. Moreover, by controlling the evaporation rate, $K$ also has a relative influence on the system's temperature and pressure [52]. Air velocity ($u_0$), another important parameter of convection drying, has no effect on the DT of the OAD system. The same result was previously observed in our

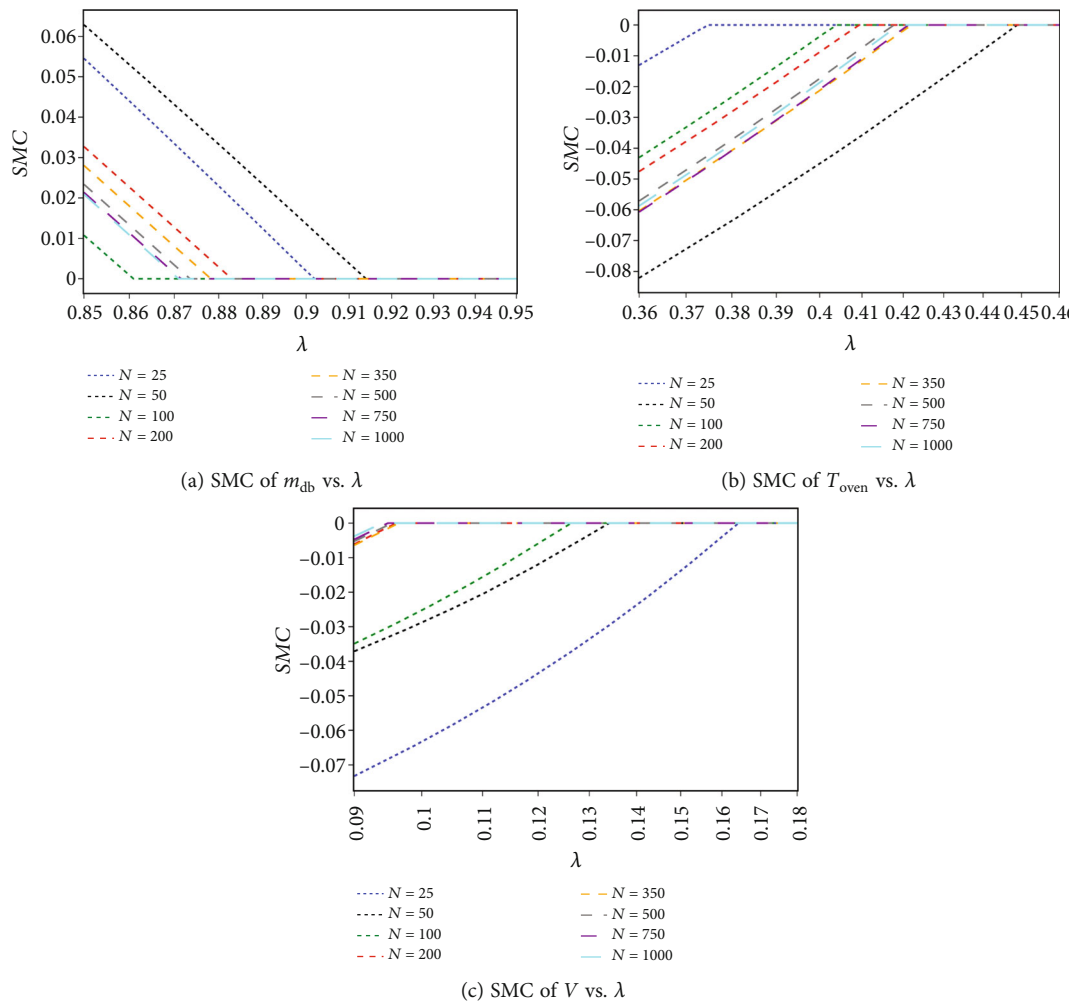


(a) SMC of $m_{db}$ vs. $\lambda$

(b) SMC of $T_{oven}$ vs. $\lambda$

(c) SMC of $V$ vs. $\lambda$

FIGURE 6: Influence of different hyperparameter ($\lambda$) values and sampling sizes ($N$) on Lasso regression (LR) model parameters for standardised model coefficient (SMC) of (a) moisture content ($m_{db}$, g water/g dry matter), (b) drying air temperature ($T_{oven}$, °C), and (c) applied voltage ($V$, V).

experimental optimisation study of the OAD system [13]. As for the other process variables, their higher values (except $m_{db,lim}$) lead to shorter DT values.

The influence of the input variables on $E_{m_{db}}$, $E_T$, and $E_P$ values of the final product is shown in Figures 7(b)–7(d). In the decreasing order, the most effective input variables are as follows:

(i) $T_{oven}$, $K$ with negative correlation, and $k_w$ with positive correlation on $E_{m_{db}}$

(ii) $T_{oven}$, $D_{eff,g}$, $K$ with positive correlation and $m_{db0}$, and $k_w$ with negative correlation on $E_T$

(iii) $D_{eff,g}$, $k_w$, and $m_{db0}$ with all negative correlations on $E_P$

The effects of these input variables on $E_{m_{db}}$, $E_T$, and $E_P$ should be investigated in terms of $\alpha$-diversity. With the simplest explanation, $\alpha$-diversity indicates the average species diversity in a habitat/specific area [41]. In our case, the term "the habitat/specific area" refers to the model geometry. And "the species" refers to the number of observations (from the output variables) that fall into each bin, as described in Section 2.4. Lower $E$ values, for example, are obtained as the number of different temperature values in the geometry increases, implying lower homogeneity. However, if all temperature values in the domain are close to each other (indicating less temperature diversity), the $E$ value is high (close to 1), as expected, indicating greater homogeneity. In terms of $E$, rather than focusing on which input variable is more efficient on homogeneity, it is important to consider whether or not ohmic heating has an effect on it. According to Figure 5, at the beginning of OAD (when ohmic heating is dominant/active), the sample homogeneity decreases from 1 to nearly half for all investigated output variables. This is because ohmic heating is a rapid heating technique that causes large variations in local temperature values as well as associated physical phenomena such as evaporation rate, internal pressure changes, and dependent transport mechanisms. As the electrical conductivity of the drying medium decreases due to the reduction in water content

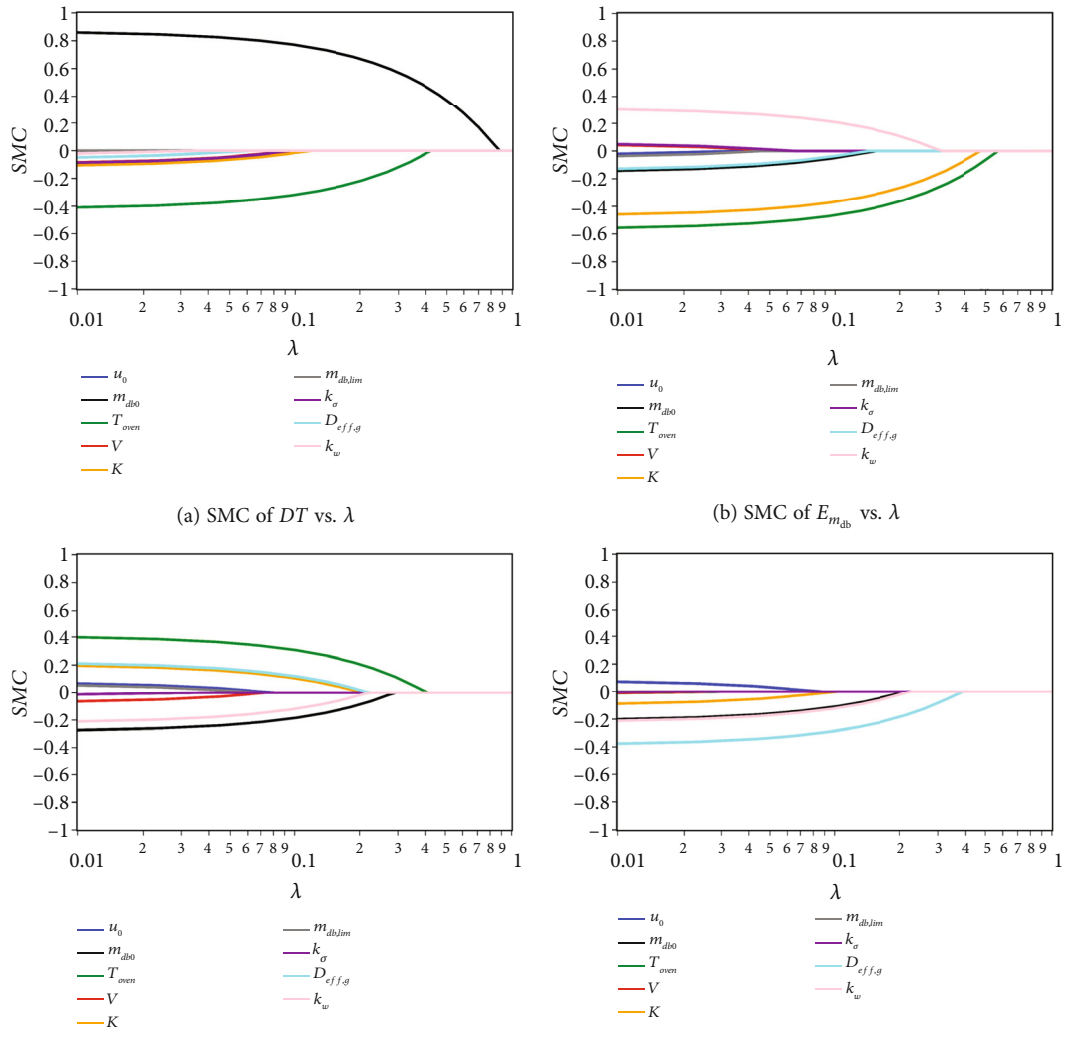


(a) SMC of $DT$ vs. $\lambda$

(b) SMC of $E_{m_{db}}$ vs. $\lambda$

(c) SMC of $E_T$ vs. $\lambda$

(d) SMC of $E_P$ vs. $\lambda$

Figure 7: Standardised model coefficients (SMCs) of Lasso regression (LR) models for (a) drying time (DT, min) and Buzas and Gibson's evenness values for (b) dry basis moisture content ($E_{m_{db}}$), (c) temperature ($E_T$), and (d) pressure ($E_P$) as output variables ($u_0$, approach velocity (m s$^{-1}$); $m_{db0}$, initial dry basis moisture content; $T_{oven}$, drying air temperature (°C); $V$, applied voltage (V); $K$, evaporation rate constant (s$^{-1}$); $m_{db,lim}$, limiting moisture for electrical conductivity; $k_\sigma$, multiplier for electrical conductivity ($\sigma$, S m$^{-1}$); $D_{eff,g}$, effective diffusion coefficient (m$^2$ s$^{-1}$); and $k_w$, multiplier for capillary diffusivity of liquid water ($D_{cap}$, m$^2$ s$^{-1}$)).

and the associated ion mobility (which is reflected in the model in the electrical conductivity dependent on water content), the influence of ohmic heating weakens and convection begins to dominate heat and mass transfer during the regular drying step. All homogeneity results belonging to the model outputs of interest rise above 0.7-0.8 and approach equilibrium towards the end of the OAD process, which is accompanied by convective drying. This means that the sample is almost homogeneous at the end. To summarise, OAD has no discernible negative impact on the spatial homogeneity of the final product. Therefore, the final product can be expected to have a similar temperature, moisture, and pressure distribution as the products produced with convection drying at the end. Furthermore, the positive effects of the OAD system on potato quality characteristics (such as colour, phenols, and enzyme inactivation) were discussed in detail in our experimental study on OAD [13].

*3.3. Time-Dependent Uncertainty.* Figures 8 and 9 depict the time-dependent effect of the model input parameters on $m_{db}$, $T$, and $P$, as well as their distribution homogeneity ($E_{m_{db}}$, $E_T$, and $E_P$). The $m_{db0}$ is by far the most efficient input factor on potato's average $m_{db}$, as well as on DT. It is the most effective parameter at the beginning of the OAD process, with a strong positive correlation between $m_{db0}$ and $m_{db}$. As drying progresses, its effect gradually diminishes and the other input variables begin to show an effect on $m_{db}$. The temperature of the sample begins to rise during the accelerated drying step, owing primarily to ohmic heating (Figure 4(b)). Thus, following $m_{db0}$, $V$ and $k_\sigma$ (the curves are superimposed on each other in Figure 8(a)) have the greatest influence on $m_{db}$. The increase in temperature causes evaporation of liquid water and thus a decrease in moisture content, which is why it correlates negatively with changes in $m_{db}$. This means that high values of $V$ and $k_\sigma$ result in higher temperatures, which

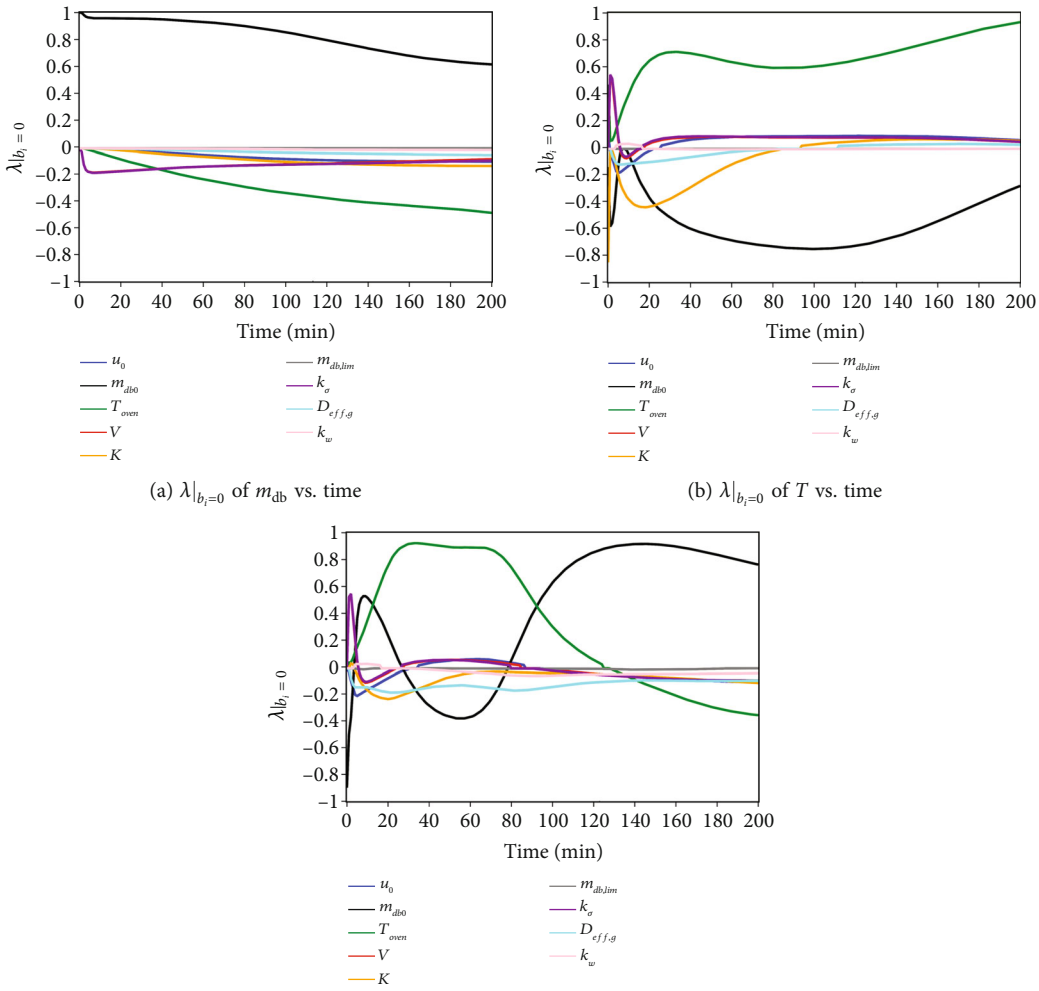


(a) $\lambda|_{b_i=0}$ of $m_{db}$ vs. time

(b) $\lambda|_{b_i=0}$ of $T$ vs. time

(c) $\lambda|_{b_i=0}$ of $P$ vs. time

FIGURE 8: $\lambda|_{b_i=0}$ (the $\lambda$ hyperparameter values that make the Lasso regression (LR) coefficients equal to zero) values from predictive LR models for (a) moisture content ($m_{db}$, g water/g dry matter), (b) temperature ($T$, °C), and (c) pressure ($P$, atm) against processing time ($u_0$, approach velocity (m s$^{-1}$); $m_{db0}$, initial dry basis moisture content; $T_{oven}$, drying air temperature (°C); $V$, applied voltage (V); $K$, evaporation rate constant (s$^{-1}$); $m_{db,lim}$, limiting moisture for electrical conductivity; $k_\sigma$, multiplier for electrical conductivity ($\sigma$, S m$^{-1}$); $D_{eff,g}$, effective diffusion coefficient (m$^2$ s$^{-1}$); and $k_w$, multiplier for capillary diffusivity of liquid water ($D_{cap}$, m$^2$ s$^{-1}$)).

promote faster evaporation. As the temperature and vapour concentration in the sample volume rise, so does the domain's overall pressure. There is no doubt that this increase creates a pressure gradient between the sample's inner regions and its boundaries, causing both liquid water and vapour to move to the boundaries via Darcy's flow and binary diffusion. Several studies on volumetric heating have previously reported similar results [31, 42, 48, 49]. The high pressure stimulates water migration from the porous structure's core to its surface [49]. High $m_{db0}$ values, on the other hand, tend to limit the increase in sample temperature because more latent heat is spent for evaporation at a high $m_{db0}$ value. According to Turgut et al. [12], a significant portion of the heat generated by electrical dissipation is used for evaporation during OAD. The electrical conductivity of the potato begins to decrease as the $m_{db}$ value of the sample decreases during drying because the medium's ability to transmit electrical current gradually decreases and disappears. As a result, the temperature and then the pressure of the medium begin to fall. Electrical dissipation, rather than convection and conduction, is the major heat mechanism in volumetric heating methods such as ohmic heating [53, 54], and the same phenomenon occurs in the OAD system, as well [12]. However, convection and conduction become stronger after ohmic heating loses its efficacy. This situation was observed in our study around the 40$^{th}$ minute of drying. According to Figure 8(a), $T_{oven}$ becomes one of the most important input variables for $m_{db}$ after this time, while the effects of $V$ and $k_\sigma$ associated with ohmic heating disappear. Apart from them, $K$, $D_{eff,g}$, and $u_0$ gain a slight importance. All these variables (except $m_{db0}$) show negative correlation with $m_{db}$. This is because higher values for all these variables help the removal moisture from the material.

A similar pattern emerges for the time-dependent uncertainty of $T$ (Figure 8(b)). $m_{db0}$, on the other hand, begins to lose its effect on $T$ after the 100$^{th}$ min of the OAD process, as

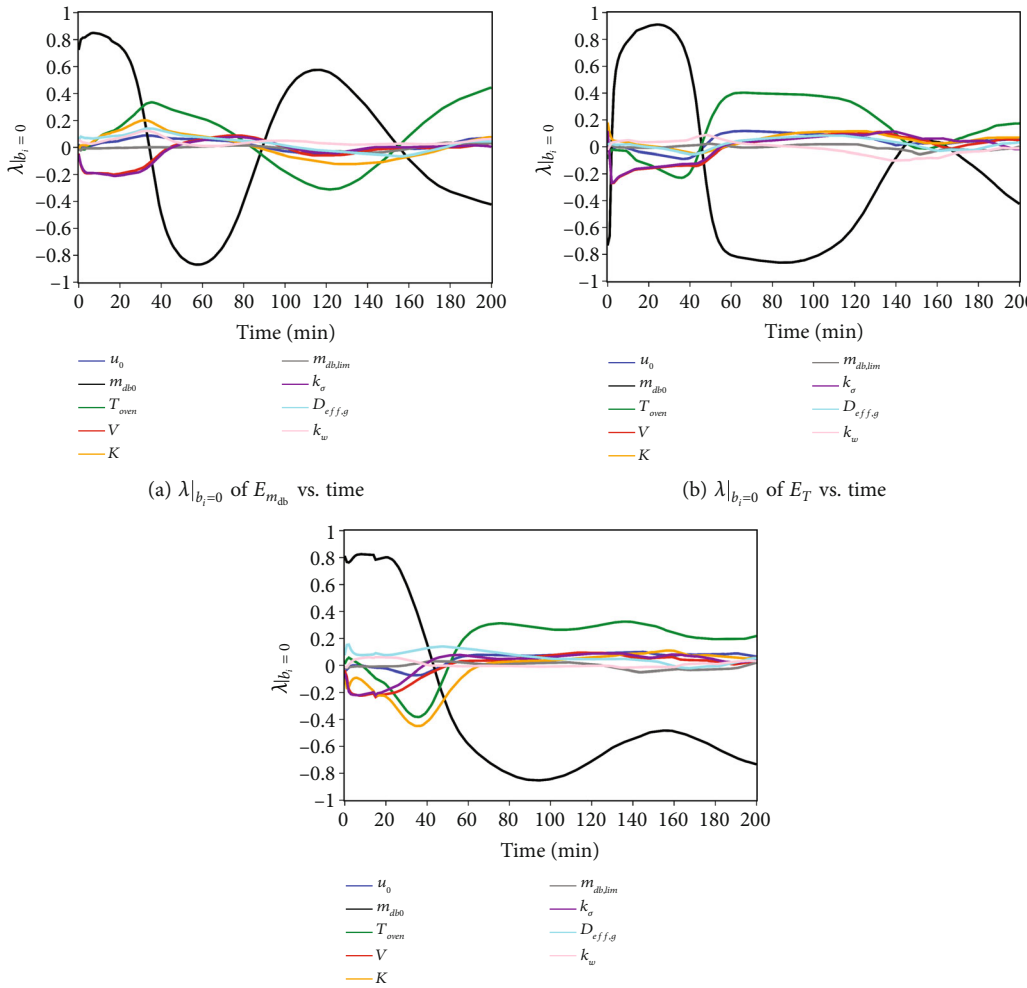


(a) $\lambda|_{b_i=0}$ of $E_{m_{db}}$ vs. time

(b) $\lambda|_{b_i=0}$ of $E_T$ vs. time

(c) $\lambda|_{b_i=0}$ of $E_P$ vs. time

FIGURE 9: $\lambda|_{b_i=0}$ (the $\lambda$ hyperparameter values that make the Lasso regression (LR) coefficients equal to zero) values from predictive LR models for Buzas and Gibson's evenness values for (a) dry basis moisture content ($E_{m_{db}}$), (b) temperature ($E_T$), and (c) pressure ($E_P$) against processing time ($u_0$, approach velocity (m s$^{-1}$); $m_{db0}$, initial dry basis moisture content; $T_{oven}$, drying air temperature (°C); $V$, applied voltage (V); $K$, evaporation rate constant (s$^{-1}$); $m_{db,lim}$, limiting moisture for electrical conductivity; $k_\sigma$, multiplier for electrical conductivity ($\sigma$, S m$^{-1}$); $D_{eff,g}$, effective diffusion coefficient (m$^2$ s$^{-1}$); and $k_w$, multiplier for capillary diffusivity of liquid water ($D_{cap}$, m$^2$ s$^{-1}$)).

is typical for convective drying [51]. This is due to a significant decrease in the sample's $m_{db}$ and the latent heat of evaporation, particularly at the sample surfaces. As a result, the heat gained from the sample by convection is mostly used to raise the temperature [12]. In the case of $P$ as an output variable, the $K$, $D_{eff,g}$, and $u_0$ appear to be other important variables after $V$, $k_\sigma$, and $T_{oven}$ (Figure 8(c)). Because these variables are also the reasons for the evaporation of liquid water and removal from surfaces. As the water vapour is removed, the $P$ value decreases proportionally. When convection becomes a dominant characteristic during the regular drying step, $T_{oven}$ becomes the most important factor for $P$ (with a positive correlation), followed by $m_{db}$ (with a negative correlation) (Figure 8(c)). The effects of these variables can be investigated from the perspective of the ideal gas law. As a result, as the oven temperature rises, the temperature of the sample (and the gases in the sample) rises as well, leading to higher internal $P$ values during the regular drying step. However, for $m_{db0}$, the situation is exactly the opposite between 20 and 80 minutes of drying in our study (Figure 8(c)). As expected, the higher the moisture content is, the more evaporation takes place, resulting in a higher pressure in the sample. However, in our study, increased evaporation (due to the ohmic heating effect during accelerated drying) results in rapid water removal, particularly due to Darcy's flow, which is not very dominant in convection drying. After the ohmic heating effect has worn off, the sample temperature decreases rapidly, causing some condensation at high voltage values. The combined effect of rapid vapour removal and cooling/condensation causes a pressure drop until the sample $T$ rises again due to convection [12]. For this reason, there is a negative relationship between $m_{db0}$ and $P$ (Figure 8(c)). However, as the evaporation rate increases after this pressure drop, $m_{db0}$ begins to have positive effect on $P$. But this time, $T_{oven}$ gradually shows a negative impact (Figure 8(c)). This is because a higher

temperature causes more heat to be transferred, resulting in a higher rate of water removal. As the amount of liquid water decreases, so does evaporation, which is the primary source of internal pressure. As a result, the internal pressure of the drying domain gradually approaches atmospheric pressure levels.

At the beginning of OAD, $m_{db0}$ is the parameter that has the most influence on the homogeneity values for $m_{db0}$, $T$, and $P$ (Figures 9(a)–9(c)). Its effects on homogeneities are all positively correlated at the start of drying (except for a very small gap for $E_T$ which can be caused by excessive initial evaporation at very high values of $m_{db0}$). Higher $m_{db0}$ values lead to higher electrical conductivity, which causes a faster temperature rise, a higher evaporation rate, and a faster pressure rise in the regions through which electric current flows. Because ohmic heating affects the entire volume, these changes take place over the majority of the sample volume and help improve homogeneity. The $D_{eff,g}$, or simply the diffusion coefficient, always tends to reduce the gradients between the regions due to its definition. Therefore, it contributes to the sample's homogeneity (Figures 9(a)–9(c)). But at the same time, the ohmic heating parameters ($V$ and $k_\sigma$) divide the model geometry into two separate parts, the hot and cold zones, due to the electrode configuration (Figure 10) [12]. This distinct separation is undoubtedly very effective in achieving low homogeneity values. In summary, $V$ and $k_\sigma$ have a negative effect on $E_{m_{db}}$, $E_T$, and $E_P$ at the beginning of OAD (Figures 9(a)–9(c)). When the ohmic heating begins to lose its effect and the regular drying step starts around the 40$^{th}$ minute of drying, the influence of $m_{db0}$ on all the homogeneity indicators turns into a negative correlation (Figures 9(a)–9(c)). Simultaneously, the influence of $T_{oven}$ and $K$ begins to grow significantly and the effects of the other input variables become slightly higher (Figures 9(a)–9(c)). At around the transition period from the accelerated drying step (when ohmic heating is active) to the regular drying step (when ohmic heating is passive), the influence of $K$ is neutralised, and it continues to follow the same trend almost until the end of the process. Around the same time, the influence of $T_{oven}$ on $E_{m_{db}}$ increases and its impact on $E_T$ and $E_P$ shifts from a negative to a positive correlation (Figures 9(a)–9(c)). This shift is the result of the dominant heat transfer mechanism changing from ohmic heating to convection. Because the inner $T$ of a potato slice (when ohmic heating is active) is notably higher than the $T$ values at the boundaries at the end of the accelerated drying step. In this context, $m_{db}$ and $P$ also exhibit a clear difference in sample volume, resulting in low homogeneity (Figures 9(a) and 9(c)). With regular drying step, $T$ of the inner regions begins to cool due to evaporation as well as heat transfer by conduction and Darcy's flow. Furthermore, convection heating causes the outer layers of the potato slice to heat up. Therefore, first $T$ and following $m_{db}$ and $P$ decrease due to similar regional differences. As a result, the homogeneity of these initial variables increases (Figures 9(a)–9(c)). After this point (approximately after the 40$^{th}$ minute of drying), the input variables affecting the homogeneity indices are $T_{oven}$ and $m_{db0}$ at different levels and in different directions. These variables, however, have no effect on the homogeneity and their values remain constant. And as already stated in Section 3.1, ohmic heating appears to not affect the final $E_{m_{db}}$, $E_T$, and $E_P$.

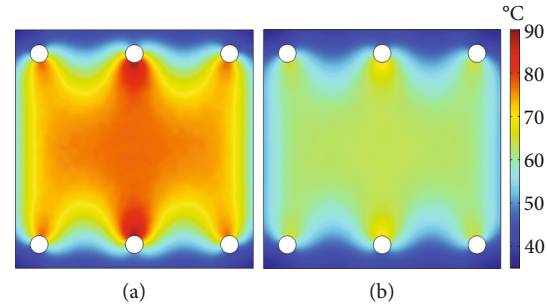


Figure 10: Predicted temperature maps of (a) interface and (b) top surface of potato slices at 5$^{th}$ min of ohmic-assisted drying where $T_{oven}$, $m_{db0}$, $u_0$, and $V$ are 60°C, 4.05, 2.15 m/s, and 100 V, respectively [12] ($T_{oven}$, drying air temperature (°C); $m_{db0}$, initial dry basis moisture content (g water/g dry matter); $u_0$, approach velocity (m s$^{-1}$); and $V$, applied voltage (V)).

*3.4. Model Refinement and Perspective.* The results of the probabilistic investigation of the OAD can be used to improve the developed mechanistic model to make better predictions and understand the possible variations in practice. According to the results of the sensitivity and uncertainty analysis of the current study, $m_{db0}$, $V$, $k_\sigma$, and $T_{oven}$ have the highest influence on all output variables (DT, $m_{db}$, $T$, $P$, $E_{m_{db}}$, $E_T$, and $E_P$). A higher $V$, $k_\sigma$, and $T_{oven}$ results in shorter DT predictions in this case. Thus, increasing $V$ and soaking pretreatment in salt solutions (to increase $k_\sigma$) improve drying performance in terms of DT. However, increasing $V$ too much can cause overshot problems at the electrode surfaces as well as undesired high heterogeneities, particularly for $m_{db}$, resulting in soggy surfaces. Intermittent current regimes at moderate voltage levels can be used to overcome these problems. At the same time, higher $T_{oven}$ values (than those used in this study) can help to reduce DT further while also resolving the heterogeneous distribution of moisture in the sample during OAD. One of the reasons for the heterogeneous moisture distribution is the accumulation of water on boundaries which is transported from the inner regions to the surfaces. This occurs when evaporation from the surfaces to the surroundings is insufficient to compensate for water transport from the sample's interior, resulting in an accumulation at the boundaries. Therefore, higher $T_{oven}$ values with higher $u_0$ can be beneficial to deal with these problems. Aside from $V$ and $T_{oven}$, $u_0$ (the third process variable controlling OAD) has no significant impact on the results not only in the present study but also in our previous experimental study [13]. However, assessing the impact of the higher $u_0$ levels above the studied range in the current study can be effective to observe its impact on OAD drying performance, and it could also be suggested as a general behaviour for convection drying. Another possible solution to overcome the heterogeneous

distribution of properties during OAD (especially to increase the spatial homogeneity and avoid overshooting) is to rearrange/improve the design and configuration of the electrodes. This results in a more homogeneous electric current distribution, as well as a homogeneous temperature, pressure, and humidity distribution.

## 4. Conclusion

The present study applies the Monte Carlo simulation approach and Lasso regression to investigate the probabilistic mechanism of hybrid system behaviours for simultaneous ohmic heating and convection drying against the combined impact of operational and model uncertainties. The input variables were ranked based on their importance/impact on stochastic model predictions and according to the results:

(1) The variables $m_{db0}$, $T_{oven}$, $V$, and $k_\sigma$ have the greatest influence on the time-dependent variation of $m_{db}$. However, there was no discernible sensitivity of $m_{db}$ to $u_0$

(2) In relation to $m_{db}$, DT is primarily influenced by $m_{db0}$, $T_{oven}$, $K$, $V$, and $k_\sigma$. To change the drying rate of materials processed with OAD, $T_{oven}$ and $V$ are required to be controlled. In addition, a treatment to increase electrical conductivity before drying (e.g., soaking in a salt solution) can help to achieve a rapid process

(3) The same parameters that affect $m_{db}$ also have an impact on the time-dependent change of $T$ and $P$ . Unlike them, $u_0$ has a very minor and ignorable impact only at the beginning of the drying process

(4) Although the magnitude and direction of $m_{db}$, $T$, and $P$'s influence on homogeneity change during drying, the main efficient input parameters on the final homogeneity properties (at the end of drying) are $m_{db0}$, $T_{oven}$, $K$, $D_{eff,g}$, and $k_w$. This demonstrates that the ohmic heating parameters ($V$ and $k_\sigma$) are not associated with the dry product's homogeneity. It is rather dependent on material and process variables

Overall, the OAD process is primarily affected by the sample's initial moisture content, oven temperature, applied voltage, and electrical conductivity. It is useful to understand how variations and changes in probabilistic input parameters affect stochastic model responses. Lasso regression is an effective method for determining the sensitivity and uncertainty of mechanistic model estimations. It can be used to assess the variance of scalar and time-dependent variables simultaneously with simple manipulation.

The findings of the current study are useful not only for researchers but also for manufacturers. These findings, for example, can be used to develop new or improved mechanistic models for OAD-based or similar systems. In this way, improving/optimising the current system can be achieved through the development of models that generate more precise predictions, and the results obtained can be used as a starting point/source of inspiration for the development of new, innovative, sustainable, and energy-efficient drying systems based on electrical energy. In addition, device manufacturers can benefit from the results of this study when designing new devices, such as a continuous OAD system. It is already known that device manufacturers use mechanistic models and Monte Carlo procedure (or similar methods) to optimise and improve their devices. The results obtained can also be used to understand and solve the reasons for the overheating and heterogeneity problems that may occur when ohmic heating-based technologies are applied to the solid food materials. To this extent, the homogeneity index derived from Buzas and Gibson's evenness value (an $\alpha$-diversity index) has, to the best of our knowledge, been introduced into the food science and technology literature. This metric is believed to be quite useful and practical for numerical evaluation of processes in terms of spatial homogeneity. Thus, this new homogeneity index will be useful not only for equipment designers but also for researchers when planning further experiments for the OAD system.

## Nomenclature

$a_w$: Water activity
$b$: LR model parameter
BC: Boundary conditions
$c_p$: Specific heat capacity ($J\,kg^{-1}\,K^{-1}$)
$D_{cap}$: Capillary diffusivity of liquid water ($m^2\,s^{-1}$)
$D_{eff,g}$: Effective diffusion coefficient ($m^2\,s^{-1}$)
DT: Drying time (min)
$E$: Buzas and Gibson's evenness value
GE: Governing equations
$h_T$: Heat transfer coefficient ($W\,m^{-2}\,K^{-1}$))
$h_m$: Mass transfer coefficient ($m\,s^{-1}$)
$H$: Shannon-Wiener diversity indices
HS: Halton sequence
$k$: Thermal conductivity ($W\,m^{-1}\,K^{-1}$)
$k_\sigma$: Multiplier for $\sigma$
$k_w$: Multiplier for $D_{cap}$
$K$: Evaporation rate constant ($s^{-1}$)
$L$: Latent heat of evaporation ($J\,kg^{-1}$)
LR: Lasso regression
$\lambda$: LR hyperparameter
$m_{db}$: Moisture content ($g\,g^{-1}$, water/dry matter, unitless)
$m_{db,lim}$: Limiting moisture for electrical conductivity
$m$: Total number of the HS samples
$\mu$: Viscosity (Pa s)
MC: Monte Carlo
MLR: Multiple linear regression
$n$: Total number of the input parameters
$N$: Number of total observations
OAD: Ohmic-assisted drying
$p_i$: Proportional value of output variables
$P$: Pressure (atm)
RSS: The sum of squared residuals

$\rho$: Density ($kg\,m^{-3}$)
SMC: Standardised model coefficient
$\sigma$: Electrical conductivity ($S\,m^{-1}$)
$t$: Time
$T$: Temperature (°C)
$T_{oven}$: Drying air temperature (°C)
$\theta$: Input variable
$u_0$: Approach velocity ($m\,s^{-1}$)
$V$: Volt (V)
$\hat{y}$: LR model output.

*Subscripts*

0: Initial value of a variable
*a*: Air
*i*: Index of MC simulations
*j*: Index of the parameter vector
*s*: Solid
*v*: Water vapour
*w*: Liquid water.

## Data Availability

The datasets generated during and/or analysed during the current study are available from the corresponding author on reasonable request.

## Additional Points

*Highlights.* (i) A probabilistic-mechanistic analysis of ohmic-assisted convectional was performed. (ii) Monte Carlo simulation with Lasso regression was used. (iii) Buzas and Gibson's evenness ($E$) was introduced as a spatial homogeneity measure. (iv) OAD performance is mostly affected by operational factors, not product properties. (v) Operational factors affect dynamic homogeneity but not sample's final homogeneity.

## Conflicts of Interest

The authors declare that they have no conflicts of interest.

## Acknowledgments

This study was funded by the "Süleyman Demirel University Scientific Research Projects Office" in Türkiye (Project ID: FDK-2019-6978). Sebahattin Serhat Turgut is also supported by a postgraduate fellowship from "The Scientific and Technical Research Council of Türkiye (TÜBİTAK)" (2211-C). The authors would like to express their gratitude to all the supporting organisations.

## Supplementary Materials

Figure S1 displays the experimental temperature maps of the top surface of potato slices for the first five minutes of OAD at different processing conditions. Additionally, Table S1 provides a concise list of assumptions, input parameters, symbols, values, and corresponding units used in the mechanistic model details detailed in Turgut et al. [12]. *(Supplementary Materials)*

## References

[1] L. Liu, Y. Wang, D. Zhao, K. An, S. Ding, and Z. Wang, "Effect of carbonic maceration pre-treatment on drying kinetics of chilli (*Capsicum annuum* L.) flesh and quality of dried product," *Food and Bioprocess Technology*, vol. 7, no. 9, pp. 2516–2527, 2014.

[2] D. Canizares and M. A. Mauro, "Enhancement of quality and stability of dried papaya by pectin-based coatings as air-drying pretreatment," *Food and Bioprocess Technology*, vol. 8, no. 6, pp. 1187–1197, 2015.

[3] S. S. Turgut, E. Küçüköner, and E. Karacabey, "Improvements in drying characteristics and quality parameters of tomato by carbonic maceration pretreatment," *Journal of Food Processing and Preservation*, vol. 42, no. 2, Article ID e13282, 2018.

[4] C. Ratti, "Hot air and freeze-drying of high-value foods: a review," *Journal of Food Engineering*, vol. 49, no. 4, pp. 311–319, 2001.

[5] G. V. Raghavan, T. J. Rennie, P. S. Sunjka, V. Orsat, W. Phaphuangwittayakul, and P. Terdtoon, "Overview of new techniques for drying biological materials with emphasis on energy aspects," *Brazilian Journal of Chemical Engineering*, vol. 22, no. 2, pp. 195–201, 2005.

[6] J. A. Moses, T. Norton, K. Alagusundaram, and B. K. Tiwar, "Novel drying techniques for the food industry," *Food Engineering Reviews*, vol. 6, no. 3, pp. 43–55, 2014.

[7] İ. Ceylan, M. Aktaş, and H. Doğan, "Apple drying at kiln by solar energy," *Journal of Polytechnic*, vol. 9, no. 4, pp. 289–294, 2006.

[8] C. Kumar, M. U. H. Joardder, T. W. Farrell, G. J. Millar, and M. A. Karim, "Mathematical model for intermittent microwave convective drying of food materials," *Drying Technology*, vol. 34, no. 8, pp. 962–973, 2016.

[9] V. H. Borda-Yepes, F. Chejne, D. A. Granados, B. Rojano, and V. S. G. Raghavan, "Mathematical particle model for microwave drying of leaves," *Heat and Mass Transfer*, vol. 55, no. 10, pp. 2959–2974, 2019.

[10] T. Defraeye and A. Martynenko, "Electrohydrodynamic drying of food: new insights from conjugate modeling," *Journal of Cleaner Production*, vol. 198, pp. 269–284, 2018.

[11] O. F. Cokgezme, S. Sabanci, M. Cevik, H. Yildiz, and F. Icier, "Performance analyses for evaporation of pomegranate juice in ohmic heating assisted vacuum system," *Journal of Food Engineering*, vol. 207, pp. 1–9, 2017.

[12] S. S. Turgut, E. Küçüköner, A. H. Feyissa, and E. Karacabey, "A novel drying system – simultaneous use of ohmic heating with convectional air drying: system design and detailed examination using CFD," *Innovative Food Science & Emerging Technologies*, vol. 72, article 102727, 2021.

[13] S. S. Turgut, E. Karacabey, and E. Küçüköner, "A novel system - the simultaneous use of ohmic heating with convective drying: sensitivity analysis of product quality against process variables," *Food and Bioprocess Technology*, vol. 15, no. 2, pp. 440–458, 2022.

[14] N. Malekjani and S. M. Jafari, "Intelligent and probabilistic models for evaluating the release of food bioactive ingredients from carriers/nanocarriers," *Food and Bioprocess Technology*, vol. 15, no. 7, pp. 1495–1516, 2022.

[15] E. Kaunisto, M. Marucci, P. Borgquist, and A. Axelsson, "Mechanistic modelling of drug release from polymer-coated and swelling and dissolving polymer matrix systems,"

*International Journal of Pharmaceutics*, vol. 418, no. 1, pp. 54–77, 2011.

[16] R. Mohammadi, M. S. Karimi, M. Raisee, and M. Sharbatdar, "Probabilistic CFD analysis on the flow field and performance of the FDA centrifugal blood pump," *Applied Mathematical Modelling*, vol. 109, pp. 555–577, 2022.

[17] S. S. Turgut, A. H. Feyissa, E. Küçüköner, and E. Karacabey, "Uncertainty and sensitivity analysis by Monte Carlo simulation: recovery of trans-resveratrol from grape cane by pressurised low polarity water system," *Journal of Food Engineering*, vol. 292, article 110366, 2021.

[18] F. Rabeler and A. H. Feyissa, "Modelling of food processes under uncertainty: mechanistic 3D model of chicken meat roasting," *Journal of Food Engineering*, vol. 262, pp. 49–59, 2019.

[19] Z. Jiang, C. Rieck, A. Bück, and E. Tsotsas, "Modeling of inter- and intra-particle coating uniformity in a Wurster fluidized bed by a coupled CFD-DEM-Monte Carlo approach," *Chemical Engineering Science*, vol. 211, article 115289, 2020.

[20] H. W. Park and W. B. Yoon, "A quantitative microbiological exposure assessment model for Bacillus cereus in pasteurized rice cakes using computational fluid dynamics and Monte Carlo simulation," *Food Research International*, vol. 125, article 108562, 2019.

[21] S. M. Gholami-Zanjani, W. Klibi, M. S. Jabalameli, and M. S. Pishvaee, "The design of resilient food supply chain networks prone to epidemic disruptions," *International Journal of Production Economics*, vol. 233, article 108001, 2021.

[22] A. H. Feyissa, K. V. Gernaey, and J. Adler-Nissen, "Uncertainty and sensitivity analysis: mathematical model of coupled heat and mass transfer for a contact baking process," *Journal of Food Engineering*, vol. 109, no. 2, pp. 281–290, 2012.

[23] E. Borgonovo and E. Plischke, "Sensitivity analysis: a review of recent advances," *European Journal of Operational Research*, vol. 248, no. 3, pp. 869–887, 2016.

[24] T. Defraeye, B. Blocken, and J. Carmeliet, "Influence of uncertainty in heat–moisture transport properties on convective drying of porous materials by numerical modelling," *Chemical Engineering Research and Design*, vol. 91, no. 1, pp. 36–42, 2013.

[25] R. L. Harrison, "Introduction to Monte Carlo simulation," *AIP Conference Proceedings*, vol. 1204, pp. 17–21, 2010.

[26] K. Cronin, "Probabilistic simulation of batch tray drying using Markov chains and the Monte Carlo technique," *Journal of Food Process Engineering*, vol. 21, no. 6, pp. 459–483, 1998.

[27] K. Cronin and S. Kearney, "Monte Carlo modelling of a vegetable tray dryer," *Journal of Food Engineering*, vol. 35, no. 2, pp. 233–250, 1998.

[28] F. Tanaka, Y. Maeda, T. Uchino, D. Hamanaka, and G. G. Atungulu, "Monte Carlo simulation of the collective behavior of food particles in pneumatic drying operation," *LWT - Food Science and Technology*, vol. 41, no. 9, pp. 1567–1574, 2008.

[29] F. Tanaka, T. Uchino, D. Hamanaka, and G. G. Atungulu, "Mathematical modeling of pneumatic drying of rice powder," *Journal of Food Engineering*, vol. 88, no. 4, pp. 492–498, 2008.

[30] H. Jaeger, A. Roth, S. Toepfl et al., "Opinion on the use of ohmic heating for the treatment of foods," *Trends in Food Science & Technology*, vol. 55, pp. 84–97, 2016.

[31] V. Rakesh, A. K. Datta, J. H. Walton, K. L. McCarthy, and M. J. McCarthy, "Microwave combination heating: coupled electromagnetics - multiphase porous media modeling and MRI experimentation," *AICHE Journal*, vol. 58, no. 4, pp. 1262–1278, 2012.

[32] Ø. Hammer, "Diversity indices," in *Paleontological Statistics Version 3.23 Reference Manual*, pp. 167-168, Oslo, 2019.

[33] J. Chen, K. Pitchai, S. Birla, M. Negahban, D. Jones, and J. Subbiah, "Heat and mass transport during microwave heating of mashed potato in domestic oven - model development, validation, and sensitivity analysis," *Journal of Food Science*, vol. 79, no. 10, pp. E1991–E2004, 2014.

[34] D. Onwude, N. Hashim, K. Abdan, R. Janius, and G. Chen, "Experimental studies and mathematical simulation of intermittent infrared and convective drying of sweet potato (*Ipomoea batatas* L.)," *Food and Bioproducts Processing*, vol. 114, pp. 163–174, 2019.

[35] C. Kumar, M. U. Joardder, T. W. Farrell, G. J. Millar, and A. Karim, "A porous media transport model for apple drying," *Biosystems Engineering*, vol. 176, pp. 12–25, 2018.

[36] A. Halder, A. Dhall, and A. K. Datta, "An improved, easily implementable, porous media based model for deep-fat frying," *Food and Bioproducts Processing*, vol. 85, no. 3, pp. 209–219, 2007.

[37] A. Kaya, O. Aydin, and I. Dincer, "Numerical modeling of forced-convection drying of cylindrical moist objects," *Numerical Heat Transfer, Part A: Applications*, vol. 51, no. 9, pp. 843–854, 2007.

[38] D. P. Kroese, T. Taimre, and Z. I. Botev, *Handbook of Monte Carlo Methods*, John Wiley & Sons, Inc., New Jersey, 2011.

[39] G. James, D. Witten, T. Hastie, and R. Tibshirani, *An Introduction to Statistical Learning with Applications in R*, Springer-Verlag, New York, 2013.

[40] M. Pyrcz, "Subsurface data analytics: the lasso for subsurface data analytics in Python," 2019 https://github.com/GeostatsGuy/PythonNumericalDemos/blob/master/SubsurfaceDataAnalytics_Lasso.ipynb.

[41] K. Özkan, *How to Measure the Components of Biodiversity (α, β ve γ)?*, Suleyman Demirel University, Isparta, Turkiye, 2016.

[42] P. Perré and I. W. Turner, "Microwave drying of softwood in an oversized waveguide: theory and experiment," *AICHE Journal*, vol. 43, no. 10, pp. 2579–2595, 1997.

[43] N. I. Lebovka, M. V. Shynkaryk, and E. Vorobiev, "Drying of potato tissue pretreated by ohmic heating," *Drying Technology*, vol. 24, no. 5, pp. 601–608, 2006.

[44] N. I. Lebovka, N. V. Shynkaryk, and E. Vorobiev, "Pulsed electric field enhanced drying of potato tissue," *Journal of Food Engineering*, vol. 78, no. 2, pp. 606–613, 2007.

[45] J. M. Bastías, J. Moreno, C. Pia, J. Reyes, R. Quevedo, and O. Muñoz, "Effect of ohmic heating on texture, microbial load, and cadmium and lead content of Chilean blue mussel (*Mytilus chilensis*)," *Innovative Food Science & Emerging Technologies*, vol. 30, pp. 98–102, 2015.

[46] E. Kamali and A. Farahnaky, "Ohmic-assisted texture softening of cabbage, turnip, potato and radish in comparison with microwave and conventional heating," *Journal of Texture Studies*, vol. 46, no. 1, pp. 12–21, 2015.

[47] F. Icier, O. F. Cokgezme, and S. Sabanci, "Alternative thawing methods for the blanched/non-blanched potato cubes: microwave, ohmic, and carbon fiber plate assisted cabin thawing," *Journal of Food Process Engineering*, vol. 40, no. 2, article e12403, 2017.

[48] C. Kumar, M. U. H. Joardder, T. W. Farrell, and M. A. Karim, "Multiphase porous media model for intermittent microwave

convective drying (IMCD) of food," *International Journal of Thermal Sciences*, vol. 104, pp. 304–314, 2016.

[49] P. Salagnac, P. Glouannec, and D. Lecharpentier, "Numerical modeling of heat and mass transfer in porous medium during combined hot air, infrared and microwaves drying," *International Journal of Heat and Mass Transfer*, vol. 47, no. 19-20, pp. 4479–4489, 2004.

[50] E. Akpinar, A. Midilli, and Y. Bicer, "Single layer drying behaviour of potato slices in a convective cyclone dryer and mathematical modeling," *Energy Conversion and Management*, vol. 44, no. 10, pp. 1689–1705, 2003.

[51] B. S. Cemeroğlu, *Drying technology, in Fruit and Vegetable Processing Technology-2*, Bizim Büro Press, Ankara, 2018.

[52] A. Halder, A. Dhall, and A. K. Datta, "An improved, easily implementable, porous media based model for deep-fat frying," *Food and Bioproducts Processing*, vol. 85, no. 3, pp. 220–230, 2007.

[53] A. Goullieux and J.-P. Pain, *Ohmic heating in Emerging Technologies for Food Processing*, D.-W. Sun, Ed., Academic Press, London, 2005.

[54] S. Jun and S. Sastry, "Modeling and optimization of ohmic heating of foods inside a flexible package," *Journal of Food Process Engineering*, vol. 28, no. 4, pp. 417–436, 2005.

[55] P. P. Lewicki, "Water as the determinant of food engineering properties. A review," *Journal of Food Engineering*, vol. 61, no. 4, pp. 483–495, 2004.

[56] F. Kaymak-Ertekin and A. Gedik, "Sorption isotherms and isosteric heat of sorption for grapes, apricots, apples and potatoes," *LWT - Food Science and Technology*, vol. 37, no. 4, pp. 429–438, 2004.